Available online at www.sciencedirect.com
ScienceDirect
Journal of Solid State Chemistry 180 (2007) 2500–2509
JOURNAL OF SOLID STATE CHEMISTRY
www.elsevier.com/locate/jssc

Solid state coordination chemistry of the oxofluorovanadium–diphosphonate system in the presence of Cu(II)–tetrapyridylpyrazine complex cations The crystal structures of $[\{Cu_2(tpyprz)(H_2O)_2\}V_4FO_8(HO_3PCH_2PO_3)_2]$, $[\{Cu_2(tpyprz)(H_2O)_2\}V_4F_6O_6(O_3PCH_2CH_2PO_3)]$, and $[Cu_2(tpyprz)\{HO_3P(CH_2)_3PO_3H\}][V_2F_2O_5]$ (tpyprz = tetra-4-pyridylpyrazine)

Wayne Ouellette[a], Vladimir Golub[b], Charles J. O'Connor[b], Jon Zubieta[a,*]

[a]Department of Chemistry, Syracuse University, Syracuse, NY 13244-4100, USA
[b]Advanced Materials Research Institute, University of New Orleans, New Orleans, LA 70148, USA

Received 9 January 2007; received in revised form 14 June 2007; accepted 20 June 2007
Available online 30 June 2007

Abstract

The hydrothermal reactions of V_2O_5, $Cu(CH_3CO_2)_2 \cdot H_2O$, tetrapyridylpyrazine (tpyprz), HF and the appropriate diphosphonic acid yielded a series of compounds of the $\{Cu^2(tpyprz)\}^{4+}/V_xO_yF_z^{n-}/\{O_3P(CH_2)_nPO_3\}^{4-}$ family of materials. The structure of $[\{Cu_2(tpyprz)(H_2O)_2\}V_4F_6O_6(HO_3PCH_2PO_3)_2]$ (**1**) is one-dimensional, constructed from mixed valence $\{V_3^{V}V^{IV}FO_8(HO_3PCH_2PO_3)_2\}^{4-}$ clusters linked through $\{Cu_2(tpyprz)(H_2O)_2\}^{4+}$ rods. The two-dimensional $[\{Cu_2(tpyprz)(H_2O)_2\}V_4F_6O_6(O_3PCH_2CH_2PO_3)]$ (**2**) is constructed from $\{V_4F_6O_6(O_3PCH_2CH_2PO_3)\}_n^{4n-}$ chains crosslinked by $\{Cu_2(tpyprz))(H_2O)_2\}^{4+}$ rods; mixed valence $\{V_2^{V}V_2^{IV}F_6O_6(O_3PCH_2CH_2PO_3)\}^{4-}$ clusters are embedded in the network. Compound **3**, $[Cu_2(tpyprz)\{HO_3P(CH_2)_3PO_3H\}][V_2F_2O_5]$, consists of $[Cu_2(tpyprz)\{HO_3P(CH_2)_3PO_3H\}]_n^{2n+}$ chains and isolated $\{V_2F_2O_5\}^{2-}$ anions. Structures **1**–**3** are compared to the structures of the analogous series $\{Cu_2(bisterpy)\}^{4+}/V_xO_yF_z^{n-}/\{O_3P(CH_2)_nPO_3\}^{4-}$, where bisterpy is 2,2′:4′:4″:2″,2‴-quaterpyridine, 6′,6″-di-2-pyridinyl. The temperature-dependent magnetic susceptibilities of **2** and **3** are also discussed.

Keywords: Bimetallic oxides; Organic–inorganic hybrid materials; Vanadium organophosphonates; Copper–tetrapyridylpyridine components; Oxyfluorovanadates

1. Introduction

Complex structures [1–6], based on a molecular scale composite of inorganic and organic components, provide the potential for the design of novel functional materials for technological applications [7]. An inorganic material may provide useful magnetic, dielectric or optical properties, mechanical hardness, and thermal stability, while organic compounds offer processability, structural diversity, a range of polarizabilities and luminescent properties [8]. Consequently, the combination of the characteristics of the organic and inorganic components offers an opportunity to conflate useful properties within a single composite, providing access to a vast area of complex, multifunctional materials [9–16].

Inorganic–organic hybrid materials [17–20] are extended arrays of metal atoms or clusters bridged by polyfunctional

*Corresponding author. Fax: +1 315 443 4070.
E-mail address: jazubiet@syr.edu (J. Zubieta).

0022-4596/$ - see front matter © 2007 Elsevier Inc. All rights reserved.
doi:10.1016/j.jssc.2007.06.020

organic molecules. An important subclass of this family of materials is the hybrid metal oxides, which contain metal–oxygen–metal (*M*–O–*M*) arrays as part of their structures. In such materials, the inorganic oxide contributes to the increased complexity, and hence functionality, through incorporation as one component in a multilevel structural material where there is a synergistic interaction between organic and inorganic components.

Metal organophosphonates are prototypical composite materials, which can exhibit a range of structures, including molecular clusters, chains, layers and three-dimensional frameworks [21–23]. An important subclass of these materials are the oxovanadium organophosphonates [24,25], whose structures are often characterized by a two-dimensional network of V–P–O layers separated by hydrophobic organic domains. However, the detailed structural chemistry may be exceedingly complex, reflecting a variety of structural determinants [26–48]. In developing the structural systematics of these materials, we have investigated the oxovanadium organodiphosphonate system, focusing on a number of variables, specifically: (i) the length and identity of the organic tether of the diphosphonates [47], (ii) the introduction of organic or metal complex cations [26,47], and (iii) the incorporation of fluoride anions into the V–P–O substructure [48,49].

Comparison of the structures of the three component oxyfluorovanadates of the $\{Cu_2(bisterpy)\}^{4+}/V_xO_yF_z^{n-}/\{O_3P(CH_2)_nPO_3\}^{4-}$ family (bisterpy = 2,2′:4′,4″:2″:2‴-quaterpyridyl-6,6″-di-2-pyridine) [48] to those of the non-fluorinated materials of the type $\{Cu_2(bisterpy)\}^{4+}/V_xO_y^{n-}/\{O_3P(CH_2)_nPO_3\}^{4-}$ reveals the profound structural consequences of fluoride incorporation. While both families exhibit anionic $\{V_xO_yF_z^{n-}\}_n$ or $\{V_xO_y^{n-}\}_n$ substructures and charge compensating complex coordination cations, the fluorinated phases manifest a considerably expanded range of V/P/O/F building blocks, including embedded clusters, chains and networks and three-dimensional frameworks. The fluorinated species also exhibited structures with V–O–V bonds in encapsulated binuclear and/or tetranuclear oxovanadium clusters, subunits which were absent in the structural chemistry of the $\{Cu_2(bisterpy)\}^{4+}/V_xO_y^{n-}$/diphosphonate family of materials.

Encouraged by these observations, we have studied the introduction of fluoride into oxovanadate–diphosphonate phases with coordination complex cation subunits other than $\{Cu_2(bisterpy)\}^{4+}$, such as the closely related, but more compact, $\{Cu_2(tpyprz)\}^{4+}$ (tpyprz = tetra-4-pyridylpyrazine). Three members of the $\{Cu_2(tpyprz)\}^{4+}/V_xO_yF_z^{n-}/\{O_3P(CH_2)_nPO_3\}^{4-}$ family, whose structures are unrelated to those observed for the $\{Cu_2(bisterpy)\}^{4+}/V_xO_yF_z^{n-}/\{O_3P(CH_2)_nPO_3\}^{4-}$ materials, were isolated: $[\{Cu_2(tpyprz)(H_2O)_2\}V_4FO_8(HO_3PCH_2PO_3)_2]$ (**1**), $[\{Cu_2(tpyprz)(H_2O)_2\}V_4F_6O_6(O_3PCH_2CH_2PO_3)]$ (**2**), and $[Cu_2(tpyprz)\{HO_3P(CH_2)_3PO_3\}][V_2F_2O_5]$ (**3**).

2. Experimental section

2.1. General considerations

All chemicals were used as obtained without further purification: copper(II) acetate monohydrate, vanadium(V) oxide, tetra-2-pyridinylpyrazine, and hydrofluoric acid (48–51%) were purchased from Aldrich; methylenediphosphonic acid was purchased from Alfa Aesar. The diphosphonate ligands 1,2-ethylenediphosphonic acid and 1,3-propylenediphosphonic acid were prepared as previously reported [50,51]. All syntheses were carried out in 23 ml poly(tetrafluoroethylene)-lined stainless steel containers under autogenous pressure. The reactants were stirred briefly, and the initial pH measured before heating. Water was distilled above 3.0 MΩ in-house using a Barnstead Model 525 Biopure Distilled Water Center. The initial and final pH of the reactions were measured using Hydrion pH sticks.

2.2. Synthesis of $[\{Cu_2(tpyprz)(H_2O)_2\}V_4FO_8(HO_3PCH_2PO_3)_2]$ (*1*)

A mixture of V_2O_5 (0.162 g, 0.891 mmol), $Cu(CH_3CO_2)_2\cdot H_2O$ (0.091 g, 0.456 mmol), tpytrz (0.087 g, 0.224 mmol), methylenediphosphonic acid (0.090 g, 0.511 mmol), H_2O (10.07 g, 559.4 mmol), and HF (0.314 g, 7.85 mmol) in the mole ratio 3.98:2.04:1.00:2.28:2497:35.04 was stirred briefly before heating to 150 °C for 168 h. Initial and final pH values of 1.5 and 1.5, respectively, were recorded. Black crystals of **1** suitable for X-ray diffraction were isolated in 15% yield. IR (KBr pellet, cm^{-1}): 3096(w), 2950(w), 1607(m), 1562(m), 1478(m), 1405(m), 1248(w), 1192(m), 1125(m), 1080(m), 996(s), 789(m), and 744(m).

2.3. Synthesis of $[\{Cu_2(tpyprz)(H_2O)_2\}V_4F_6O_6\{O_3P(CH_2)_2PO_3\}]$ (*2*)

A solution of V_2O_5 (0.082 g, 0.451 mmol), $Cu(CH_3CO_2)_2\cdot H_2O$ (0.089 g, 0.446 mmol), tpytrz (0.086 g, 0.221 mmol), 1,2-ethylenediphosphonic acid (0.064 g, 0.337 mmol) H_2O (10.01 g, 556.1 mmol), and HF (0.555 g, 13.88 mmol) in the mole ratio 2.04:2.02:1.00:1.52:2516:62.81 was stirred briefly before heating to 150 °C for 72 h (initial and final pH values were 1.0 and 1.0, respectively). Black crystals of **2** suitable for X-ray diffraction were isolated in 90% yield. IR (KBr pellet, cm^{-1}): 3068(w), 1597(m), 1476(m), 1411(m), 1296(w), 1261(w), 1191(m), 1111(s), 1045(m), 965(s), 785(m), and 760(m).

2.4. Synthesis of $[\{Cu_2(tpyprz)\}\{HO_3P(CH_2)_3PO_3H\}][V_2F_2O_5]$ (*3*)

A solution of V_2O_5 (0.082 g, 0.451 mmol), $Cu(CH_3CO_2)_2\cdot H_2O$ (0.090 g, 0.451 mmol), tpytrz (0.086 g, 0.221 mmol), 1,3-propylenediphosphonic acid (0.093 g, 0.456 mmol), H_2O (10.02 g, 556.7 mmol) and HF (0.150 g, 3.75 mmol)

in the mole ratio 2.04:2.04:1.00:2.06:2519:16.97 was heated at 140 °C for 72 h (initial and final pH: 2.5 and 2.0, respectively). Green crystals of **3** suitable for X-ray diffraction were isolated in 50% yield. IR (KBr pellet, cm^{-1}): 3068(w), 1472(w), 1422(m), 1198(s), 1058(m), 968(m), 884(m), 805(m), 789(m), and 632(m).

2.5. X-ray crystallography

Crystallographic data for all compounds were collected with a Brücker P4 diffractometer equipped with a SMART CCD system [52] and using Mo$K\alpha$ radiation ($\lambda = 0.71073$ Å). The data were collected at 90 K and corrected for Lorentz and polarization effects. Absorption corrections were made using SADABS [53]. The structure solutions and refinements were carried out using the SHELXTL [54] crystallographic software package. The structures were solved using direct methods, and all of the non-hydrogen atoms were located from the initial solution. After locating all of the non-hydrogen atoms in each structure, the models were refined against F^2, initially using isotropic then anisotropic thermal displacement parameters, until the final value of Δ/σ_{max} was less than 0.001. Hydrogen atoms with the exception of those associated with water molecules of crystallization, which were not included either at observed or calculated positions, were located at calculated positions and included in the final cycles of refinement using a riding model. The fluorine positions were unambiguously identified from observations of the behavior of the temperature factors and refinements of the occupancy factors of the oxygen and fluorine sites. With a sound, low-temperature data set and a well-behaved structure, fluorine and oxygen sites are readily distinguished. As an example of the power of X-ray crystallography to provide chemical analysis by atomic displacement parameters, see Ref. [55], which demonstrates the principle for the more difficult case of Al vs. Si occupancies. Crystallographic data for the structure solutions and refinements of compounds **1–3** are summarized in Table 1. Selected bond lengths and angles for compounds **1–3** are provided in Tables 2–4, respectively.

2.6. Magnetism

Magnetic data were recorded on 17–25 mg samples of compound in the 2–300 K temperature range using a Quantum Design MPMS-5S SQUID spectrometer. Calibrating and operating procedures have been reported previously [56]. The temperature-dependent data were obtained at a magnetic field of $H = 1000$ Oe.

3. Results and discussion

3.1. Synthesis and infrared spectroscopy

Conventional hydrothermal methods [57–60] have been demonstrated to provide suitable conditions for the preparation and crystallization of organic–inorganic hybrid materials [60]. For compounds **1–3**, heating a mixture of V_2O_5, $Cu(CH_3CO_2)_2 \cdot H_2O$, tetrapyridylpyrazine, HF and the appropriate diphosphonate in water at 140–150 °C for 72 h provided black or green crystals in variable yields. It is noteworthy that crystalline products were obtained only with $Cu(CH_3CO_2)_2 \cdot H_2O$ as the copper source. Attempts to prepare materials of the $\{Cu(tpyprz)\}^{4+}/V_xO_yF_z^{n-}/\{O_3P(CH_2)_nPO_3\}^{4-}$ for $n > 3$ were unsuccessful.

The use of HF as a mineralizer to improve solubility and crystal growth in oxovanadium-based organic–inorganic hybrid materials is common. While in most cases fluoride is not incorporated into the product, oxyfluorinated products have been reported upon adjustment of the HF/V ratio [61,62]. In this case, at low HF/V ratios (5:1 or less), no fluorine incorporation into the copper vanadate products was observed. However, at increased HF/V ratios of 8:1 or greater, the oxyfluoride materials of this study were isolated.

Although the V(V) starting material V_2O_5 was used in the synthesis of **1–3**, the products **1** and **2** were mixed valence V(IV)/V(V) materials, as suggested by their dark green/black color. The reduction of V(V) to V(IV), and even to V(III), is quite common in the presence of nitrogenous ligands [63].

The infrared spectra of **1–3** are characterized by a group of three or four bands of medium to strong intensity in the 1000–1500 cm^{-1} range associated with the diphosphonate ligand. In addition, a strong band in the 960–1000 cm^{-1} region is attributed to υ(V=O).

3.2. X-ray crystal structures

As shown in Fig. 1, the structure of **1** is constructed from $\{V_4FO_8(HO_3PCH_2PO_3)_2\}^{4-}$ clusters linked through $\{Cu_2(tpyprz)(H_2O)_2\}^{4+}$ clusters into a one-dimensional zig-zag chain. Each vanadium site is six coordinate, bonding to a terminal oxo-group, two μ^2-oxo-groups, the central μ^{4-} fluoride of the cluster, and an oxygen donor from each of two $\{HO_3PCH_2PO_3\}^{3-}$ ligands. Each diphosphonate ligand bridges four vanadium sites and links to a copper(II) site of the $\{Cu_2(tpyprz)(H_2O)_2\}^{4+}$ cluster. One oxygen site of each diphosphonate ligand is pendant and protonated. The structure may alternatively be described as a $\{V_4O_4\}$ ring with a central fluoride group and four terminal oxo-groups, that is, a $\{V_4FO_8\}^{2+}$ cluster capped by two diphosphonate ligands.

The copper sites exhibit square pyramidal geometry, with the basal plane defined by three nitrogen donors of the binucleating tpyprz ligand and the Cu–O–V bridging oxo-group and the apical position occupied by an aqua ligand. Charge balance considerations imply that the cluster is a mixed valence $V^V_3V^{IV}$ species. Valence sum calculations [64] on the vanadium sites of the cluster provide an average valence of 4.68, compared to a theoretical average valence of 4.75 for a $V^V_3V^{IV}$ species. The valence sum calculation

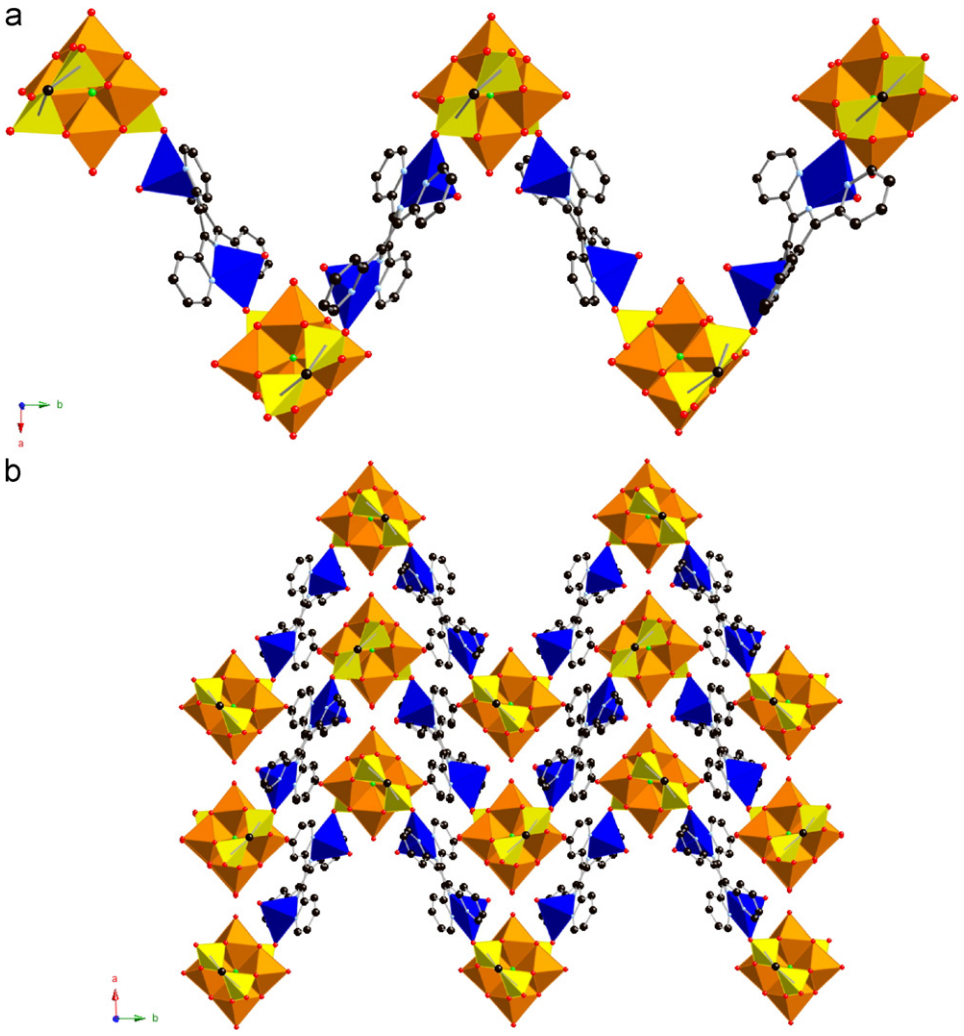

Fig. 1. (a) Polyhedral representation of the one-dimensional structure of [{Cu_2(tpyprz)(H_2O)$_2$}V_4FO_8($HO_3PCH_2PO_3$)$_2$] (**1**) and (b) the packing of chains in the *ab* plane.

implies that the electron of the d^1 V(IV) site is delocalized about the ring.

The structure of **2**, illustrated in Fig. 2, is two-dimensional, consisting of chains of {$V_4F_6O_6$($O_3PCH_2CH_2PO_3$)}$^{4-}$ clusters linked through the diphosphonate ligands which are in turn crosslinked through the {Cu_2(tpyprz)(H_2O)$_2$}$^{4+}$ units. The oxofluorovanadium clusters consist of four edge-sharing {VF_3O_3} octahedra. Two of the octahedra are defined by a doubly bridging fluoride, a triply bridging fluoride, a terminal fluoride, a doubly bridging oxo-group, a terminal oxo-group and an oxygen donor from the diphosphonate ligand. The two remaining vanadium octahedra exhibit two triply bridging fluorides, a doubly bridging fluoride, a doubly bridging oxo-group, a terminal oxo-group and an oxygen donor from the diphosphonate ligand. The fluoride donors adopt a *facial* configuration about the vanadium centers of either type.

Each diphosphonate ligand contributes two oxygen donors from one {O_3P} terminus to one vanadium cluster and two oxygen donors from the second {O_3P} terminus to an adjacent vanadium cluster; the remaining oxygen donor at each phosphorus site is used to connect to a {Cu_2(tpyprz)(H_2O)$_2$}$^{4+}$ unit.

The square pyramidal geometry at the Cu(II) sites is again defined by three tpyprz nitrogen donors and the Cu–O–V bridging oxo-group in the basal plane and an apical aqua ligand. Charge balance stipulates that the cluster of **2** is a mixed valence $V^V_2V^{IV}_2$ species. In contrast to the electronic delocalization observed for **1**, the valence sums for the vanadium sites of **2** establish the V(1) site as the V(V) site and the V(2) site as V(IV).

The contrasting dimensionalities of **1** and **2** are consistent with bonding patterns previously established for diphosphonate ligands [49,65]. Thus, the methylenediphosphonate ligand does not possess the spatial extension to span adjacent clusters so as to generate chain motifs of the type {–cluster–$O_3PCH_2PO_3$–}$_n$, but rather adopts chelating modes with a single metal site or bridging geometries to metal sites of a single cluster. Consequently, spatial expansion in one-dimension is accomplished in **1** through the {Cu_2(tpyprz)(H_2O)$_2$}$^{4+}$ rods. In contrast, the

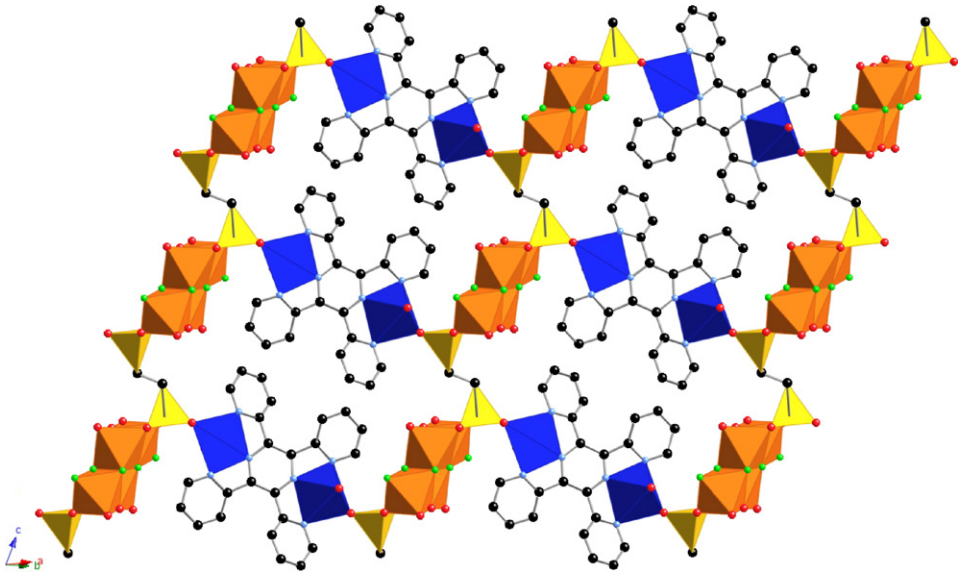

Fig. 2. Polyhedral representation of the two-dimensional structure of $[\{Cu_2(tpyprz)(H_2O)_2\}V_4F_6O_6(O_3PCH_2CH_2PO_3)]$ (**2**).

Table 1
Summary of crystallographic data for the structures of $[Cu_2(tpyprz)(H_2O)_2V_4FO_8(O_3PCH_2PO_3)_2]$ (**1**), $[Cu_2(tpyprz)(H_2O)_2V_4F_6O_6(O_3P(CH_2)_2PO_3)]$ (**2**), and $[\{Cu_2(tpyprz)\}\{HO_3P(CH_2)_3PO_3H\}][V_2F_2O_5]$ (**3**)

	1	**2**	**3**
Empirical formula	$C_{13}H_{13}CuF_{0.50}N_3O_{11}P_2V_2$	$C_{13}H_{12}CuF_3N_3O_7PV_2$	$C_{13.50}H_{12}CuFN_3O_{5.50}PV$
fw	624.12	575.65	468.71
Cryst syst	Orthorhombic	Triclinic	Monoclinic
Space group	*Pnna*	P-1	*C*2/*c*
a (Å)	18.7085(11)	9.8529(10)	14.1395(7)
b (Å)	19.5216(11)	10.1438(10)	12.3301(6)
c (Å)	10.3967(6)	10.4442(10)	17.5892(8)
α (deg)	90	78.814(2)	90
β (deg)	90	66.044(2)	98.4780(10)
γ (deg)	90	64.306(2)	90
V (Å^3)	3797.1(4)	859.41(15)	3033.0(3)
Z	8	2	8
D_{calcd} (g cm^{-3})	2.184	2.225	2.053
μ (mm^{-1})	2.317	2.464	2.174
T (K)	90	90	90
λ (Å)	0.71073	0.71073	0.71073
R_1[a]	0.0624	0.0373	0.0272
wR_2[b]	0.1232	0.0820	0.0705

[a] $R_1 = \Sigma|F_o - |F_c|/\Sigma|F_o|$.
[b] $wR_2 = \{\Sigma[w(F_o^2 - F_c^2)^2]/\Sigma[w(F_o^2)^2]^{1/2}\}$; $w = 1/[\sigma^2(F_o^2) + (a \times P)^2 + b \times P]$; $P = [\mathrm{Max}(F_o^2, 0) + 2F_c^2]/3$.

ethylenediphosphonate ligand readily bridges cluster sites to provide a one-dimensional {–cluster–$O_3PCH_2CH_2PO_3$–} substructure. In this case, the $\{Cu_2(tpyprz)(H_2O)_2\}^{4+}$ subunit may be exploited to link adjacent chains to produce a two-dimensional architecture.

To our surprise, the structure of **3** consists of one-dimensional $\{Cu_2(tpyprz)(HO_3PCH_2CH_2CH_2PO_3H)\}_n^{2n+}$ chains and isolated $\{V_2F_2O_5\}^{2-}$ anion clusters (Fig. 3). The copper–diphosphonate chain consists of $\{Cu_2(tpyprz)\}^{4+}$ rods linked through $\{HO_3P(CH_2)_3PO_3H\}^{2-}$ ligands. The copper sites exhibit square pyramidal $\{CuN_3O_2\}$ geometry. Each binuclear copper(II) unit is linked to two adjacent copper substructures through three diphosphonate ligands. In turn, each diphosphonate bridges three $\{Cu_2(tpyprz)\}^{4+}$ groups. Each $\{HO_3P\}$ terminus of the diphosphonate ligand provides an oxygen donor to each of two $\{Cu_2(tpyprz)\}^{4+}$ rods, leaving a pendant, protonated oxygen site.

The $\{V_2F_2O_5\}^{2-}$ cluster consist of two corner-sharing V(V) tetrahedra. Each tetrahedron is defined by two terminal oxo-groups, a bridging oxo-group and a terminal fluoride. The gross features of the cluster are similar to those of the well-documented $\{V_2O_7\}^{4-}$ cluster which also exhibits corner-sharing tetrahedron [25,66].

The most unusual characteristic of structures **1**–**3** is the identification of a unique cluster embedded within each,

Table 2
Selected bond lengths (Å) and angles (deg) for $[Cu_2(tpyprz)(H_2O)_2V_4FO_8(HO_3PCH_2PO_3)_2]$ (**1**)

Cu(1)–O(1)	1.898(3)
Cu(1)–N(2)	1.956(3)
Cu(1)–N(3)	2.018(4)
Cu(1)–N(1)	2.020(3)
Cu(1)–O(90)	2.291(3)
V(1)–O(4)	1.612(4)
V(1)–O(5)#1	1.865(3)
V(1)–O(5)	1.865(3)
V(1)–O(2)	1.949(3)
V(1)–O(2)#1	1.949(3)
V(1)–F(1)	2.273(3)
Σvs	4.69
V(2)–O(6)	1.602(3)
V(2)–O(7)	1.855(3)
V(2)–O(5)	1.885(3)
V(2)–O(8)	1.959(3)
V(2)–O(3)	1.974(3)
V(2)–F(1)	2.2327(7)
Σvs	4.68
V(3)–O(10)	1.599(5)
V(3)–O(7)#1	1.863(3)
V(3)–O(7)	1.863(3)
V(3)–O(9)#1	1.974(3)
V(3)–O(9)	1.974(3)
V(3)–F(1)	2.296(3)
Σvs	4.66
O(1)–Cu(1)–N(2)	169.19(14)
N(3)–Cu(1)–N(1)	157.96(14)
O(1)–Cu(1)–O(90)	103.71(13)
O(5)#1–V(1)–O(5)	150.63(18)
O(2)–V(1)–O(2)#1	166.59(18)
O(4)–V(1)–F(1)	180.0
O(7)–V(2)–O(5)	152.37(13)
O(8)–V(2)–O(3)	168.05(12)
O(6)–V(2)–F(1)	179.19(15)
O(7)#1–V(3)–O(7)	149.41(18)
O(9)#1–V(3)–O(9)	167.49(17)
O(10)–V(3)–F(1)	180.0
V(2)–F(1)–V(2)#1	178.93(17)
V(2)–F(1)–V(1)	90.53(8)
V(2)#1–F(1)–V(1)	90.53(8)
V(2)–F(1)–V(3)	89.47(8)
V(2)#1–F(1)–V(3)	89.47(8)
V(1)–F(1)–V(3)	180.0
P(1)–O(1)–Cu(1)	134.87(18)
P(1)–O(2)–V(1)	133.75(18)
P(1)–O(3)–V(2)	133.08(18)
V(1)–O(5)–V(2)	117.24(14)
V(2)–O(7)–V(3)	118.03(15)
P(2)–O(8)–V(2)	134.30(18)
P(2)#1–O(9)–V(3)	132.65(18)

Symmetry transformations used to generate equivalent atoms: #1 x, $-y+1/2$, $-z+1/2$; #2 $-x+1/2$, $-y+1$, z.

Table 3
Selected bond lengths (Å) and angles (deg) for $[Cu_2(tpyprz)(H_2O)_2V_4F_6O_6(O_3P(CH_2)_2PO_3)]$ (**2**)

Cu(1)–O(1)	1.8999(16)
Cu(1)–N(2)	1.9653(19)
Cu(1)–N(3)	1.999(2)
Cu(1)–N(1)	2.005(2)
Cu(1)–O(90)	2.2276(18)
V(1)–O(5)	1.5909(17)
V(1)–O(4)	1.7277(17)
V(1)–O(2)#1	1.9259(16)
V(1)–F(1)	1.9520(14)
V(1)–F(3)	2.0332(16)
V(1)–F(1)#1	2.3010(14)
Σvs	4.83
V(2)–O(3)	1.5967(17)
V(2)–F(3)	1.8613(16)
V(2)–F(2)	1.8857(14)
V(2)–O(4)#1	1.9752(17)
V(2)–O(6)	2.0004(17)
V(2)–F(1)	2.2614(14)
Σvs	4.20
O(1)–Cu(1)–N(2)	169.24(8)
N(3)–Cu(1)–N(1)	159.12(8)
O(2)#1–V(1)–F(1)	154.21(7)
O(4)–V(1)–F(3)	157.84(7)
O(5)–V(1)–F(1)#1	174.78(7)
F(2)–V(2)–O(4)#1	157.28(7)
F(3)–V(2)–O(6)	153.01(7)
O(3)–V(2)–F(1)	174.33(8)
V(1)–F(1)–V(2)	98.62(6)
V(1)–F(1)–V(1)#1	106.59(6)
V(2)–F(1)–V(1)#1	87.65(5)
V(2)–F(3)–V(1)	110.48(8)
P(1)–O(1)–Cu(1)	138.39(11)
P(1)–O(2)–V(1)#1	127.23(10)
V(1)–O(4)–V(2)#1	116.97(9)
P(1)–O(6)–V(2)	137.37(10)

Symmetry transformations used to generate equivalent atoms: #1 $-x+1,-y+1,-z+1$; #2, $-x$, $-y$, $-z+1$.

either as an anionic building block or as an isolated anion. Furthermore, the structural chemistry of the $\{Cu_2(tpyprz)\}^{4+}/V_xO_yF_z^{n-}/\{O_3P(CH_2)_nPO_5\}^{4-}$ series contrasts dramatically with that of the previously described $\{Cu_2(bisterpy)\}^{4+}/V_xO_yF_z^{n-}/\{O_3P(CH_2)_nPO_3\}^{4-}$ family of materials. This latter series features six structures constructed from mononuclear $\{VO_xF_y\}^{n-}$ units, three with embedded binuclear $\{V_2O_xF_y\}^{n-}$ constituents and a single structure $[\{Cu_2(bisterpy)\}_3V_8F_6O_{17}\{HO_3P(CH_2)_3PO_3\}_4]$ with a tetranuclear building block. As shown in Fig. 4, the $\{V_4FO_8(HO_3PCH_2PO_3)_2\}^{4-}$ unit of **1**, the $\{V_4F_6O_6(O_3PCH_2CH_2PO_3)\}^{4-}$ substructure of **2**, and the $[V_4F_4O_8\{HO_3P(CH_2)_3PO_3\}_2]^{6-}$ cluster of $[\{Cu_2(bisterpy)\}_3V_8F_6O_{17}\}$ are quite distinct in terms of polyhedral types and connectivities, as well as vanadium oxidation states.

The dramatic structural differences between the $\{Cu_2(tpyprz)\}^{4+}/V_xO_yF_z^{n-}/\{O_3P(CH_2)_nPO_3\}^{4-}$ and $\{Cu_2(bisterpy)\}^{4-}/V_xO_yF_z^{n-}/\{O_3P(CH_2)_nPO_3\}^{4-}$ families is somewhat surprising since the only difference in the components is the ligand. However, bisterpy and tpyprz are similar tridentate heterocyclic ligand types, and $\{Cu_2(bisterpy)\}^{4+}$ and $\{Cu_2(tpyprz)\}^{4+}$ are analogous building blocks but for the Cu···Cu distances, as illustrated in Fig. 5. The contrasting structures of the two series of materials illustrates once again the dramatic consequences of small variations in the component

building block on the overall architectures and even dimensionalities of the products.

We had also noted previously that while the cluster chemistry of oxofluorovanadates exhibits high V:F ratios of 4:1–6:1, the solid phases are clustered about lower V:F ratios of 1:1–2:1. However, compound **1** of this study exhibits an unusually high V:F ratio for a solid phase of 4:1, while compound **2** shows a similarly low V:F ratio of 1:1.5. Similarly, the O:F ratios for previously described solid phases fall in the range 1:1–4:1. While compounds **2** and **3** fall within this common range (1:1 and 1:2.5, respectively), compound **1** exhibits an O:F ratio of 8:1. The O:F ratios of the solid phases suggest that charge matching considerations may set natural limits on the extent to which fluoride with a −1 charge may substitute for oxide (−2) in the construction of complex oxyfluorides of vanadium.

Table 4
Selected bond lengths (Å) and angles (deg) for [{Cu_2(tpyprz)}{$HO_3P(CH_2)_3PO_3H$}][$V_2F_2O_5$] (**3**)

Cu(1)–O(1)	1.8982(11)
Cu(1)–N(2)	1.9710(13)
Cu(1)–N(3)	2.0359(13)
Cu(1)–N(1)	2.0577(13)
Cu(1)–O(2)	2.1353(11)
V(1)–O(6)	1.6193(13)
V(1)–O(4)	1.6466(13)
V(1)–F(3)	1.7850(11)
V(1)–O(5)	1.8024(5)
O(1)–Cu(1)–N(2)	170.91(5)
N(3)–Cu(1)–N(1)	149.91(5)
O(6)–V(1)–O(4)	108.66(7)
O(6)–V(1)–F(3)	108.78(7)
O(4)–V(1)–F(3)	109.76(7)
O(6)–V(1)–O(5)	111.60(7)
O(4)–V(1)–O(5)	110.70(6)
F(3)–V(1)–O(5)	107.30(4)
P(1)#1–O(1)–Cu(1)	131.51(7)
P(1)–O(2)–Cu(1)	133.62(7)
V(1)–O(5)–V(1)#2	149.57(11)

Symmetry transformations used to generate equivalent atoms: #1, $-x$, $-y+1$, $-z+1$; #2, $-x$, y, $-z+1/2$.

3.3. Magnetic susceptibility studies

Magnetic measurements were collected for compounds **2** and **3**. The temperature dependence of the magnetic susceptibility and the effective magnetic moment for **2** is shown in Fig. 6. The formulation of **2** implies that there are four magnetic ions with ($S=\frac{1}{2}$), two Cu(II) and two V(IV) sites. The best fit to the data was obtained using a combination of the Heisenberg dimer model ($S=\frac{1}{2}$) for the V(IV) ions and the Curie–Weiss law for the Cu(II) centers:

$$\chi = \frac{N_A g_V^2 \mu_B^2}{k_B T} \frac{2\exp((2J)/k_B T)}{1+3\exp((2J)/k_B T)} + \frac{N_A g_{Cu}^2 \mu_B^2}{2k_B(T-\theta)} + \chi_{TI}. \quad (1)$$

The best fit was $g_v = 1.96$, $g_{Cu} = 2.02$, $J/k_B = -9.5\,K$, $\theta = 2.1\,K$, · and $\chi_{TI} = -0.00055\,cm^3/mol$. The effective magnetic moment at 300 K is 2.60 μ_B. The analysis provided is a simplification of the magnetic exchange in this material. However, the general expression for the magnetic susceptibility of this complex system would require at least seven free fitting parameters, which cannot be extracted from the experimental data. In order to reduce the number of parameters, a simplified model, giving an approximation of the exchange phenomena, was adopted. Attempts to use more realistic models produced ambiguity in the parameters.

The results of magnetic measurements on **3** are shown in Fig. 7. The presence of a maximum in the magnetic susceptibility at ca. 45 K indicates the presence of antiferromagnetic coupling between the Cu(II) sites. Two magnetic pathways are possible: through the π-system of the tpyprz ligand or through the {$Cu_2(O_3PCH_2CH_2PO_3)$} bridges of the chain. Although strong antiferromagnetic

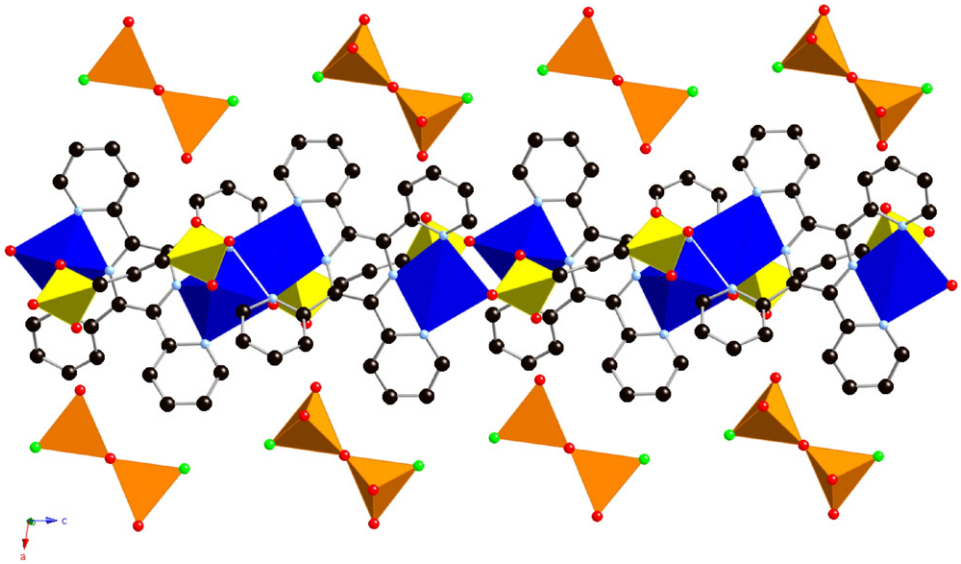

Fig. 3. Polyhedral view of the structure of [{Cu_2(tpyprz)}{$HO_3P(CH_2)_3PO_3H$}][$V_2F_2O_5$] (**3**).

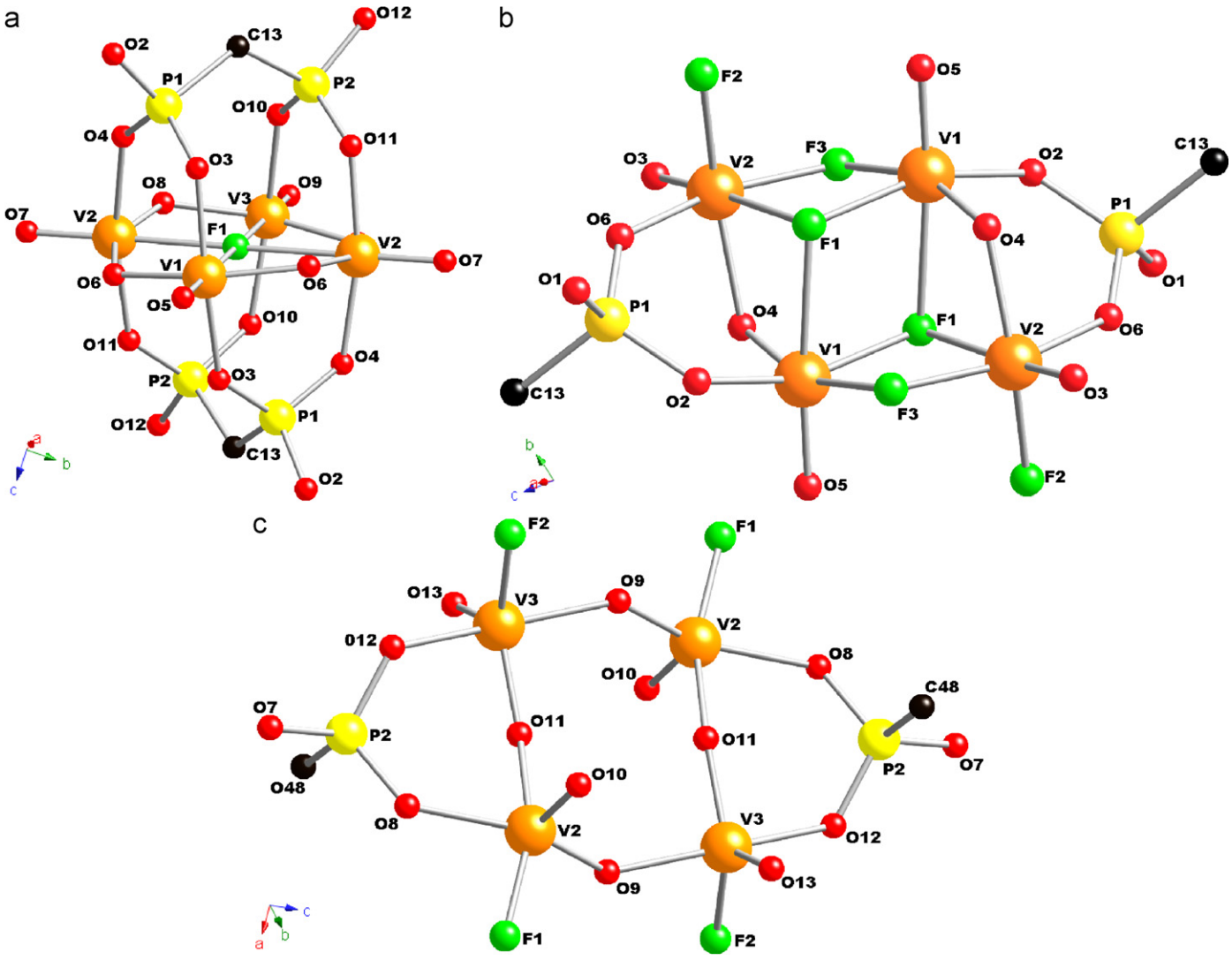

Fig. 4. Ball and stick models of the embedded tetranuclear clusters of (a) **1**, (b) **2**, and (c) $[\{Cu_2(bisterpy)\}_3V_8F_6O_{17}\{HO_3P(CH_2)_3PO_3\}_4]$, showing the atom-labeling schemes.

coupling is generally not observed for copper sites of $\{Cu_2(bisterpy)\}^{4+}$ and $\{Cu_2(tpyprz)\}^{4+}$ [48] units (Cu···Cu distances of 10.85 and 6.55 Å, respectively), the phosphonate bridges produce a Cu···Cu distance of 10.08 Å and seem unlikely pathways for magnetic exchange [67–69].

The best description of the experimental results for **3** were obtained using the Heisenberg dimer model ($S = \frac{1}{2}$) taking into account the presence of monomeric paramagnetic impurities with concentration x:

$$\chi = (1-x)\frac{N_A g_V^2 \mu_B^2}{k_B T}\frac{2\exp((2J)/k_B T)}{1+3\exp((2J)/k_B T)} + x\frac{N_A g_{Cu}^2 \mu_B^2}{2k_B(T-\theta)} + \chi_{TI}. \quad (2)$$

The best fit was $g = 2.19$, $J/k_B = -36$ K, $\chi_{TI} = -0.00124\,cm^3/mol$, and $x = 0.015$. The effective magnetic moment at 300 K is 2.60 μ_B.

4. Conclusions

Hydrothermal chemistry has effected the isolation of three members of the $\{Cu_2(tpyprz)\}^{4+}/V_xO_yF_z^{n-}/\{O_3P(CH_2)_nPO_3\}^{4-}$ family of materials. Compound **1** $[\{Cu_2(tpyprz)(H_2O)_2\}V_4FO_8(HO_2PCH_2PO_3)_2]$ is one-dimensional and contains the unusual mixed valence $\{V_4FO_8(H)_3PCH_2PO_3)_2\}^{4-}$ cluster as a building block. In contrast, compound **2** $[\{Cu_2(tpyprz)(H_2O)_2\}V_4F_6O_6(O_3PCH_2CH_2PO_3)]$ is two-dimensional and is constructed from a distinct mixed valence tetranuclear cluster $\{V_4F_6O_6(O_3PCH_2CH_2PO_3)\}^{4-}$. The structure of compound **3**, $[Cu_2(tpyprz)\{HO_3P(CH_2)_3PO_3H\}][V_2F_2O_5]$, consists of one-dimensional $[Cu_2(tpyprz)\{HO_3P(CH_2)_3PO_3H\}]_n^{2n+}$ chains and isolated $\{V_2F_2O_5\}^{2-}$ anionic clusters. The structures of **1**–**3** reveal three novel oxyfluorovanadium cluster building blocks.

It is noteworthy that the structures of the $\{Cu_2(tpyprz)\}^{4+}/V_xO_yF_z^{n-}/\{O_3P(CH_2)_nPO_3\}^{4-}$ family exhibit

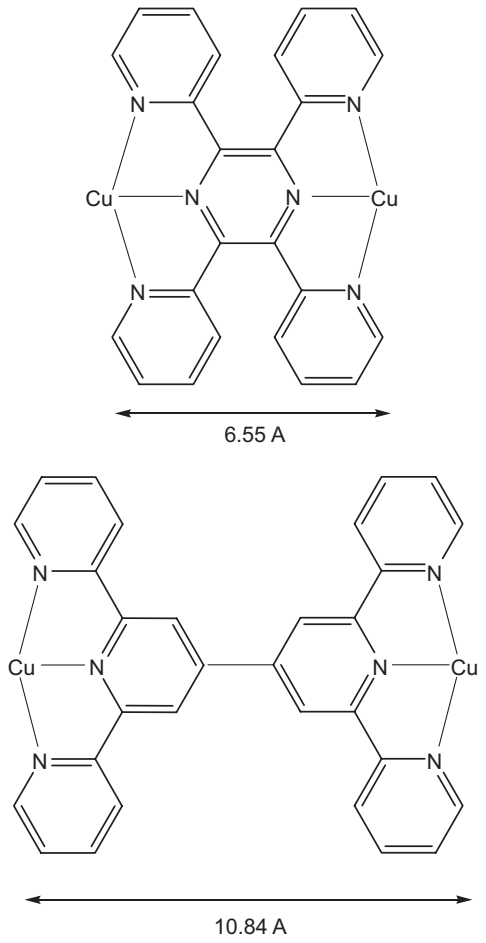

Fig. 5. Schematic representations of $\{Cu_2(tpyprz)\}^{4+}$ and $\{Cu_2(bisterpy)\}^{4+}$, showing the Cu · · · Cu distances.

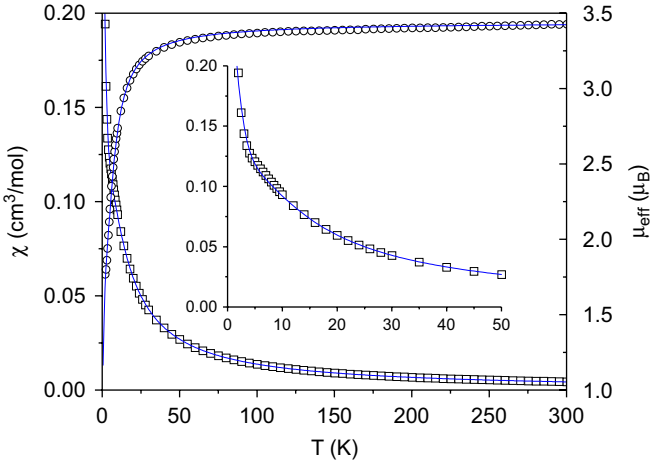

Fig. 6. Temperature dependence of the magnetic susceptibility χ (□) and the effective magnetic moment μ_{eff} (○) of **2**. The lines drawn through the data points are the fits to Eq. (1).

different component building blocks and consequently overall architectures from those of the analogous $\{Cu_2(bisterpy)\}^{4+}/V_xO_yF_z^{n-}/\{O_3P(CH_2)_nPO_3\}^{4-}$ family. The principles that govern the self-assembly of the

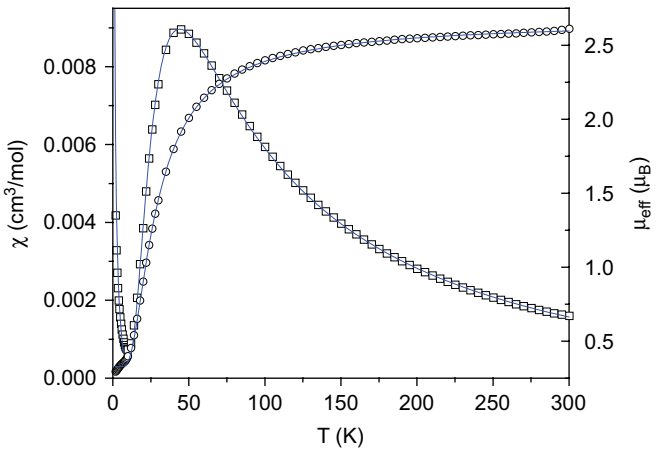

Fig. 7. Temperature dependence of the magnetic susceptibility χ (□) and the effective magnetic moment μ_{eff} (○) of **3**. The lines drawn through the data points are the fits to the Heisenberg dimer model, Eq. (2).

constituent building blocks of these complex materials remain elusive. However, the complexity of hydrothermal parameter species in combination with variations in polyhedral types for the metals, polyhedral connectivities and aqua ligation, with the "softness" of the M–O–P angles, with variable protonation of phosphonate groups, with apparently promiscuous substitution of fluoride for oxide and with unpredictable reduction of vanadium sites results in an unusual structural diversity. We continue to explore the influence of systematic changes in pH, temperature, and stoichiometry, as well as geometric factors such as the length and rigidity of the organic components.

5. Supplementary materials

CCDC Nos. 631615–631617 contain the supplementary crystallographic data for compounds **1**–**3**. These data can be obtained free of charge via http://www.ccdc.cam.ac.uk/conts/retrieving.html, or from the Cambridge Crystallographic Data Centre, 12 Union Road, Cambridge CB2 1EZ, UK; fax: +44 1223 336 033; or e-mail: deposit@ccdc.cam.ac.uk

Acknowledgments

This work was supported by a grant from the National Science Foundation, CHE-0604527 and by the Defense Advances Research Projects Agency (MDA972-04-1-0029).

References

[1] Complexity is a subject of significant and general scientific interest. Complexity in chemistry refers to the description and manipulation of systems of molecules, as in living cells and materials. In the latter context, organic–inorganic hybrid structures partake of the chemical complexity of materials, with the attendant complications of predictability and rational design. See, for example: G.M. Whitesides, R.F. Ismagilov, Science 284 (1999) 89.

[2] The relationship between complexity and functionality is abundantly evident in biological systems. Chemists may learn from biology and make the creative leap to the design of inorganic materials whose structures are influenced by organic molecules. See, for example: I.Z. Kiss, J.L. Hudson, AICLE J. 49 (2003) 2234 and references [3–6].
[3] J.M. Lehn, Proc. Natl. Acad. Sci. 99 (2002) 4763.
[4] J.M. Lehn, Science 295 (2002) 2400.
[5] S. Förster, T. Plantenberg, Angew. Chem. Int. Ed. Engl. 41 (2002) 688.
[6] A.D. Miller, Chem. Biochem. 3 (2002) 45.
[7] C. Janiak, Dalton Trans. (2003) 2781 and references therein.
[8] D.B. Mitzi, Dalton Trans. (2001) 1.
[9] The properties of inorganic–organic hybrids, specifically metal-organic frameworks (MOF) have been extensively elaborated in recent years B. Chen, N.W. Ockwig, A.R. Millward, S.D. Contreras, O.M. Yaghi, Angew. Chem. Int. Ed. Eng. 44 (2005) 4745 and references [10–16].
[10] D. Bradshaw, J.B. Claridge, E.J. Cussen, T.J. Prior, M.J. Rosseinsky, Chem. Res. 38 (2005) 273.
[11] O. Ohmori, M. Kawano, M. Fujita, Angew. Chem. Int. Ed. 44 (2005) 1962.
[12] C.-D. Wu, W. Lin, Angew. Chem. Int. Ed. 44 (2005) 1958.
[13] A.C. Sudik, A.R. Millward, N.W. Ockwig, A.P. Cote, J. Kim, O.M. Yaghi, J. Am. Chem. Soc. 127 (2005) 7110.
[14] R. Kitaura, S. Kitagawa, Y. Kubtoa, T.C. Kobayashi, K. Kindo, Y. Mita, A. Matsuo, M. Kobayashi, H.-C. Chang, T.C. Ozawa, M. Suzuki, M. Sakata, M. Takata, Science 298 (2002) 2358.
[15] D. Bradshaw, T.J. Prior, E.J. Cussen, J.B. Claridge, M.J. Rosseinsky, J. Am. Chem. Soc. 126 (2004) 6106.
[16] G.J. Halder, C.J. Kepert, B. Moubaraki, K.S. Murray, J.D. Cashion, Science (Washington, DC, US) 298 (2002) 1762.
[17] A.K. Cheetham, C.N.R. Rao, R.K. Feller, Chem. Commun. (2006) 4780.
[18] S. Kitagawa, S. Noro, Compr. Coordinat. Chem. II 7 (2004) 231.
[19] C.N.R. Rao, S. Natarajan, R. Vaidhyanathan, Angew. Chem. Int. Ed. 43 (2004) 1466.
[20] O.M. Yaghi, M. O'Keeffe, N.W. Ockwig, H.K. Chae, M. Eddaoudi, J. Kim, Nature 423 (2003) 705.
[21] A. Clearfield, Curr. Opin. Solid State Mater. Sci. 6 (2003) 495.
[22] A. Clearfield, Prog. Inorg. Chem. 47 (1998) 371.
[23] G. Alberti, in: J.L. Atwood, J.E.D. Davis, F. Vogel (Eds.), Comprehensive Supramolecular Chemistry, vol. 9, Pergamon Press, New York, 1996, p. 182.
[24] R.C. Finn, J. Zubieta, R.C. Haushalter, Prog. Inorg. Chem. 51 (2003) 451.
[25] M.I. Khan, J. Zubieta, Prog. Inorg. Chem. 43 (1995) 1.
[26] W. Ouellette, B.-K. Koo, E. Burkholder, V. Golub, C.J. O'Connor, J. Zubieta, Dalton Trans. (2004) 1527.
[27] M. Riou-Cavellec, M. Sanselme, G. Férey, J. Mater. Chem. 10 (2000) 745.
[28] G. Huan, J.W. Johnson, A.J. Jacobson, J.S. Merola, J. Solid State Chem. 89 (1990) 220.
[29] W.T.A. Harrison, L.L. Dussack, A.J. Jacobson, Inorg. Chem. 35 (1996) 1461.
[30] M.I. Khan, Y.-S. Lee, C.J. O'Connor, R.S. Haushalter, J. Zubieta, Inorg. Chem. 33 (1994) 3855.
[31] M.I. Khan, Y.-S. Lee, C.J. O'Connor, R.S. Haushalter, J. Zubieta, Chem. Mater. 6 (1994) 4525.
[32] M.I. Khan, Y.-S. Lee, C.J. O'Connor, R.S. Haushalter, J. Zubieta, Chem. Mater. 6 (1994) 721.
[33] V. Soghomonian, Q. Chen, R.C. Haushalter, J. Zubieta, Agnew. Chem., Int. Ed. Engl. 34 (1995) 4460.
[34] V. Soghomonian, R. Diaz, R.C. Haushalter, C.J. O'Connor, J. Zubieta, Inorg. Chem. 34 (1995) 4460.
[35] V. Soghomonian, R.C. Haushalter, J. Zubieta, Chem. Mater. 7 (1995) 1648.
[36] G. Bonavia, R.C. Haushalter, C.J. O'Connor, J. Zubieta, Inorg. Chem. 35 (1996) 5603.
[37] C. Ninclaus, C. Serre, D. Riou, G. Férey, C. R. Acad. Sci. Paris Ser. IIc 1 (1998) 551.
[38] G. Bonavia, R.C. Haushalter, S. Lu, C.J. O'Connor, J. Zubieta, J. Solid State Chem. 132 (1997) 144.
[39] D. Riou, C. Serre, G. Férey, J. Solid State Chem. 141 (1998) 89.
[40] D. Riou, O. Roubeau, G. Férey, Microporous Mesoporous Mater. 23 (1998) 23.
[41] D. Riou, G. Férey, J. Mater. Chem. 8 (1998) 2733.
[42] G. Yucesan, V. Golub, C.J. O'Connor, J. Zubieta, Dalton Trans. (2005) 2241.
[43] G. Yucesan, V. Golub, C.J. O'Connor, J. Zubieta, Solid State Sci. 7 (2005) 133.
[44] G. Yucesan, W. Ouellette, V. Golub, C.J. O'Connor, J. Zubieta, Solid State Sci. 7 (2005) 445.
[45] G. Yucesan, M.H. Yu, W. Ouellette, C.J. O'Connor, J. Zubieta, Cryst. Eng. Commun. 7 (2005) 480.
[46] G. Yucesan, M.-H. Yu, C.J. O'Connor, J. Zubieta, Cryst. Eng. Commun. 7 (2005) 711.
[47] W. Ouellette, M.H. Yu, J.C. O'Connor, J. Zubieta, Inorg. Chem. (2006) 3224.
[48] W. Ouellette, V. Golub, C.J. O'Connor, J. Zubieta, Dalton Trans. 20 (2005) 291.
[49] W. Ouellette, M.H. Yu, C.J. O'Connor, J. Zubieta, Inorg. Chem. 45 (2006) 7628.
[50] D.I. Arnold, X. Ouyang, A. Clearfield, Chem. Mater. 14 (2002) 2020.
[51] J.C. Horne, C.J. Blanchard, J. Am. Chem. Soc. 118 (1996) 12788.
[52] Bruker-AXS, SMART Software, Version 5.630, Siemens Analytical X-ray Instruments, Inc., Madison, WI, 1994.
[53] G.M. Sheldrick, SADABS: Program for Empirical Absorption Corrections, University of Göttingen, Göttingen, Germany, 1996.
[54] G.M. Sheldrick, SHELXTL-Plus: Program for Refinement of Crystal Structures: Version 6.14, Bruker-AXS, Madison, WI, USA, 1996.
[55] C.L. Condron, H. Hope, P.M.B. Piccoli, A.J. Schultz, S.M. Kauzlarich, Inorg. Chem. 46 (2007) 4523.
[56] C.J. O'Connor, Prog. Inorg. Chem. 29 (1979) 203.
[57] M.S. Whittingham, Curr. Opin. Solid State Mater. Sci. 1 (1996) 227.
[58] R.A. Laudise, Chem. Eng. News 65 (1987) 30.
[59] A.N. Lobachev, Crystallization Processes Under Hydrothermal Conditions, Consultants Bureau, New York, 1973.
[60] J. Gopalakrishnan, Chem. Mater. 7 (1995) 1265.
[61] J. Zubieta, Solid State Methods, Hydrotherm. Compr. Coordinat Chem. II 1 (2004) 697.
[62] D. Riou, G. Férey, J. Solid State Chem. 111 (1994) 422.
[63] C. Ninclaus, D. Riou, G. Férey, Chem. Commun. (1997) 851.
[64] N.E. Breese, M. O'Keeffe, Acta Crystallogr. Sect. B 47 (1991) 192.
[65] E. Burkholder, V. Golub, C.J. O'Connor, J. Zubieta, Inorg. Chem. 43 (2004) 7014.
[66] P.J. Hagrman, R.C. Finn, J. Zubieta, Solid State Sci. 3 (2001) 745.
[67] R.C. Haushalter, Q. Chen, V. Soghomonian, J. Zubieta, C.J. O'Connor, J. Solid State Chem. 108 (1994) 128.
[68] D. Beltran-Porter, A. Beltran-Porter, P. Amoros, R. Ibanez, G. Martinez, A. LeBail, G. Férey, G. Villeneuve, Eur. J. Solid State Chem. 28 (1991) 131.
[69] G. Villeneuve, P. Amoros, D. Beltran, M. Drillen, Organic and inorganic low dimensional crystalline materials, in: P. Delkaes, M. Drillen (Eds.), NATO Asi Series, vol. B168, Plenum Press, New York, 1987, p. 417.